Analysis of Battery-Supercapacitor Hybrid Energy Storage System with MPC-based PMSM Control for Electric Vehicles

***Abstract*—The devastating impacts of climate change have become increasingly evident in recent decades, with the key responsible sources being the emission of greenhouse gases (GHGs) such as carbon dioxide CO_2 and sulfur dioxide SO_2. A significant proportion of greenhouse gases (GHGs) originate from the tailpipe emissions of conventional vehicles. Fortunately, electric vehicles (EVs) being a zero carbon transport, have emerged as a potential solution to mitigate the repercussions associated with conventional vehicles. However, there are a few major shortcomings of EVs which include a limited driving range, battery degradation and the technical challenges related to developing a robust and efficient Energy Management System (EMS). To address these issues, this paper presents the design of a rule-based EMS for a semi-active Hybrid Energy Storage System (HESS) consisting Battery and Supercapacitors (SCs) by implementing a smart algorithm that harnesses the regenerating braking for battery charging and optimizes power delivery from the HESS. Additionally, a Model Predictive Control (MPC) method is employed to control the speed of the Permanent Magnet Synchronous Motor (PMSM) of EV. The complete model has been designed and analyzed in MATLAB/Simulink environment under specified conditions and the overall response has been thoroughly studied. The simulation outcomes suggest that the proposed system is capable of enhancing energy efficiency, improving power quality as well as stability, and extending the battery lifespan.**

***Index Terms*—Energy Management System (EMS), Hybrid Energy Storage System (HESS), Supercapacitor (SC), Semi-active Topology, Model Predictive Control (MPC).**

I. Introduction

The most ruinous effect of conventional vehicles on the environment is the emission of various noxious gases such as nitrogen oxides (NO_X), carbon monoxide (CO), carbon dioxide (CO_2), sulfur dioxide (SO_2) and other greenhouse gases (GHGs). A study in 2014 states that, the transportation sector was responsible for 23% of the planet's total emitted CO_2 gas [1]. Between 1990 and 2016, New Zealand's total increase in GHG emissions from transportation was 71.3% wherein 90.7% of these emissions were from road transport. The increase in transport emissions during that period was 58.8% and 21.3% in Australia and USA respectively [2]. These statistics reveal the dominance of the percentage share of GHG emissions solely from conventional vehicles on the road.

For the past few decades, EVs have proved to be a viable option in protecting our environment and combating climate change. As countries worldwide target a low-carbon economy, EVs are playing a critical role in transportation decarbonization. Generally, EVs can be categorized broadly into three types such as: Battery Electric Vehicle (BEV), Hybrid Electric Vehicle (HEV) and Plug-in Hybrid Electric Vehicle (PHEV). The primary energy storage element and the driving force for an EV is the battery. Among numerous types of batteries, Lithium-ion (Li-ion) battery is the most widely used battery owing to its fast-charging ability, compact size, and low maintenance requirements [3]–[5].

While the battery in EVs possesses a high energy density that enables it to supply energy throughout a driving mission, the battery is adversely affected by other significant operations of EVs, including sudden acceleration and deceleration [4]–[6]. Additionally, the frequent charging and discharging of the battery in EVs to meet their power demands contributes to battery aging [7]. Typically, charging an EV to full capacity takes long hours which can be extremely inconvenient for the daily drivers [8]. With the increased number of charge cycles and temperature fluctuations, the performance of Li-ion batteries degrade leading to reduced driving range and battery lifetime [9]. The cost of replacing an EV battery pack can be quite high and battery disposal has a detrimental impact on the environment too [10].

To address these limitations effectively, a promising solution involves integrating batteries and supercapacitors (SCs) in a coupled system. SCs inherently having high power density are the perfect storage element for serving the dynamic power needs of EVs. They can be charged and discharged thousands of times without affecting performance, allowing for enhanced transient performance and extended battery longevity. Moreover, SCs have the capability of receiving high currents from regenerative braking that contributes to increased driving range. Thus, a combination of battery and SC that forms a Hybrid Energy Storage System (HESS) is attracting researchers since HESS blends the benefits of both battery and SC [6]. However, efficiently connecting the SCs and battery to the DC link poses a significant challenge in

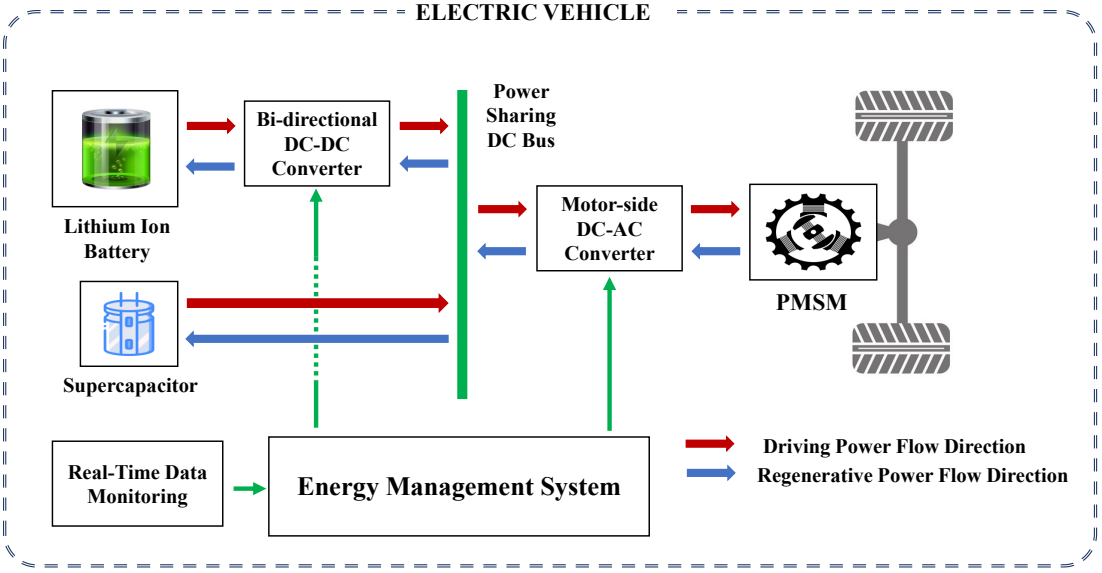

Fig. 1. Schematic diagram of Energy Management System in an Electric Vehicle.

the implementation of a HESS. Semi-active HESS topology refers to a configuration where energy storage components, such as batteries and SCs, are interconnected through a DC-DC bidirectional converter. A robust EMS centrally controls the power flow among various powertrain components such as batteries, SCs, DC-DC converters, inverters, motors, and more [11].

In this paper, a battery and SC-based semi-active HESS has been designed and simulated for EV. The proposed HESS comprises a Li-ion battery and a SC bank consisting of 100 series-connected SCs, each connected to a DC link bus. For managing the power flow optimally, a rule-based EMS has been designed that ensures synergy between the battery and SCs. An intelligent algorithm has been incorporated into the proposed rule-based EMS that can produce power by harnessing regenerative braking. Finally, an MPC-based motor controller has been established for controlling the speed of the 10 kW, 3-phase PMSM of the EV. The complete model has been designed and simulated in MATLAB/Simulink environment and a performance analysis has been conducted in this study.

II. Methodology

In this section, the proposed Hybrid Energy Storage System (HESS), Energy Management System (EMS) and Model Predictive Control (MPC) based PMSM control techniques will be discussed in detail. The schematic diagram of the system is depicted in Fig. 1.

A. Proposed Semi-active Hybrid Energy Storage System

The proposed HESS has been developed based on semi-active topology, which comprises a 265 V, 100 Ah Li-ion battery connected to a bidirectional dc-dc converter, and a 300 V, 10 F SC-bank of 100 SCs directly connected to the DC link bus. The operation of the dc-dc converter is governed to meet the smooth high power demand component. This control is achieved by supplying control pulses to the converter, which are generated based on the filtered reference power demand obtained through the application of an adaptive filtering algorithm [12]. The inverter converts the DC power from the power-sharing bus to AC power, which drives the Permanent Magnet Synchronous Motor (PMSM). Model Predictive Control (MPC), a sophisticated control technique known for its predictive capabilities, is implemented to regulate the operation of the PMSM with precise control. The parameter values and descriptions of the components in the model are provided in Table I.

B. Rule-based Energy Management System Algorithm

The energy management system (EMS) proposed in this study aims to address the power demand by utilizing both Li-ion battery and SC technologies. Specifically, the rule-based strategy focuses on utilizing the battery to fulfill the high-power and consistent portion of the demand, while the fluctuating part of the demand is handled by the SCs, as shown in Fig 2.

TABLE I
Specifications of Proposed Electric Vehicle Model

Component	Description	Value
Lithium-ion Battery	Nominal Voltage	265 V
	Capacity	100 Ah
	Initial State of Charge	50 %
Supercapacitor Bank	Nominal Voltage	300 V
	Capacitance	10 F
	No. of series connected	100
	Rated Current	30 A
PMSM	Rated Power	10 kW
	Rated Speed	2300 rpm
	Rated Torque	41.4 N.m
DC-Link	Voltage	300 V

To achieve this, a low-pass filtering algorithm is adapted to extract the smoother part from the reference demand power. The transfer function of the low-pass filter can be expressed as [12]:

$$G(s) = \frac{1}{\tau s + 1} \tag{1}$$

where τ is the time constant of the low-pass filter.

To mitigate abrupt changes and preserve demand power integrity, a rate limiter algorithm is applied. It involves computing the difference between the current input sample $x(n)$ and the previous output sample $y(n-1)$, expressed as:

$$\Delta y(n) = x(n) - y(n-1) \tag{2}$$

This difference $\Delta y(n)$ is then used to find the output $y(n)$.

$$y(n) = \begin{cases} y(n-1) + \Delta y(n) & \text{if } |\Delta y(n)| \leq L \cdot Ts \\ y(n-1) + \text{sign}(\Delta y(n)) \cdot L \cdot Ts & \text{otherwise} \end{cases} \tag{3}$$

where L is the rate limit and Ts is the sampling period.

In practical scenarios, there are cases where the SCs need to be charged in parallel with the motor power consumption, particularly when the SCs have a low charge level. Alternatively, the SCs may be tasked with supplying high power demand when the battery state of charge is nearing depletion [13]. To effectively manage this issue, four distinct cases of different battery State of Charge (SoC) and SC Charge Level (CL) statuses have been proposed in Table II [14].

TABLE II
PROPOSED CASES FOR BATTERY AND SC CHARGE STATUS

Case	Battery SoC Status (%)	SC CL Status (%)
1	30 – 100	80 – 100
2	30 – 100	0 – 80
3	0 – 30	60 – 100
4	0 – 30	0 – 60

Case 1: In this case, both the battery and the SCs will supply power to the motor. The battery supplies only the smoother portion of the power demand (P_{bat} = P_d) while SCs are responsible to fully support the fluctuating portion of the power demand (P_{SC} = P_f) of the motor. During regenerative braking, only the power flow direction is reversed.

Case 2: For this case, the battery charges the SC and also supplies power to the motor. The amount of power supplied by the battery, P_{bat} is given by Equation 4. The amount of power supplied by the supercapacitors, P_{SC} is calculated by Equation 5. The constant factor ($\frac{212}{CL}$) in both equations is selected based on the equivalence of the Li-ion battery's storage capacity to about 212 times that of the SCs. This approach is employed to transfer the power from the battery to the SCs based on their respective charging levels.

$$P_{bat} = P_d + 2 \cdot SoC_{bat} \cdot \frac{212}{CL_{SC}} \tag{4}$$

$$P_{SC} = P_f - 2 \cdot SoC_{bat} \cdot \frac{212}{CL_{SC}} \tag{5}$$

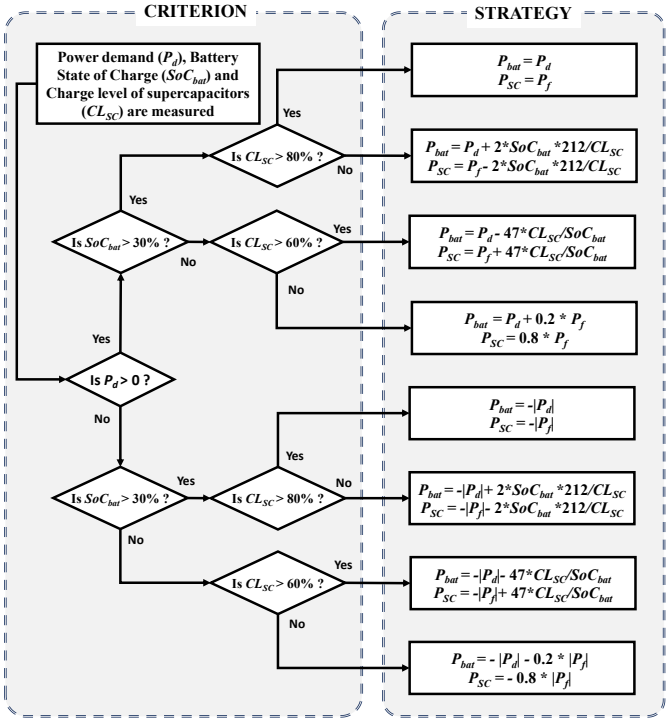

Fig. 2. Flowchart of the proposed rule-based EMS algorithm.

Case 3: In this scenario, the battery supplies less power than the power demand of the motor and receives more power from regenerative braking. The amount of power supplied by the battery, P_{bat} and supercapacitors, P_{SC} is estimated by Equation 6 and 7, respectively. To accommodate the considerable difference in storage capacity between SCs and batteries, the charging power from the SC to the battery is reduced by approximately five times compared to the scenario where the battery charges the SCs.

$$P_{bat} = P_d - \frac{47 \cdot \text{CL}_{SC}}{SoC_{bat}} \tag{6}$$

$$P_{SC} = P_f + \frac{47 \cdot \text{CL}_{SC}}{SoC_{bat}} \tag{7}$$

Case 4: For this case, both the battery and SCs contribute power to the motor, with the battery supporting a small proportion (20%) and SCs remaining proportion (80%) of the fluctuating power. Power levels of battery, P_{bat} and Supercapacitors, P_{SC} are computed using Equation 8 and 9, respectively. During regenerative braking, the battery receives the majority of the energy since it serves as the primary energy storage for the vehicle.

$$P_{bat} = P_d + 0.2 \cdot P_f \tag{8}$$

$$P_{SC} = 0.8 \cdot P_f \tag{9}$$

Once the battery power requirement is generated through the algorithm, the control pulse is generated by utilizing a PID controller. This control pulse is then supplied to the

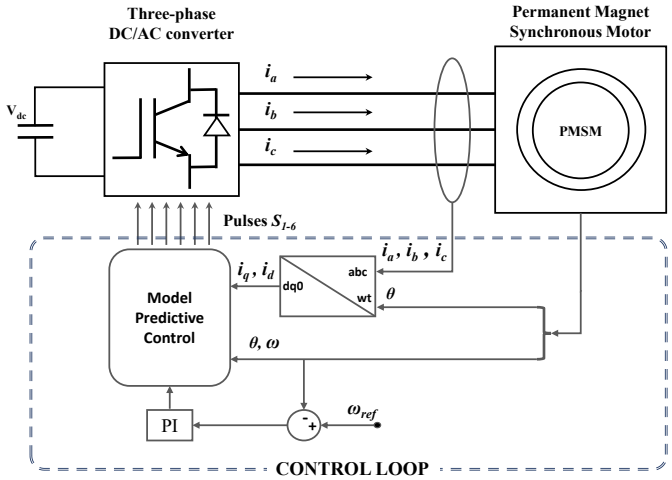

Fig. 3. Schematic diagram of model predictive control system.

bidirectional buck-boost converter in order to regulate the power flow.

C. PMSM Speed Regulation by Model Predictive Control

The speed of the PMSM of the EV is regulated by MPC technique. The schematic diagram and the control loop of the MPC system is displayed in Fig. 3. To control the motor speed, the model takes the reference signals for motor speed and stator current as inputs and provides the switching pulses to the inverter. The control scheme is designed in the two-phase d-q frame, which is obtained from the three-phase stator currents using the Park transformation. The Park transformation converts the three-phase stator current into two-phase d-q axis current as follows [14]:

$$\begin{bmatrix} i_d \\ i_q \end{bmatrix} = \frac{2}{3} \begin{bmatrix} \cos(\theta) & \cos(\theta - 2\pi/3) & \cos(\theta + 2\pi/3) \\ -\sin(\theta) & -\sin(\theta - 2\pi/3) & -\sin(\theta + 2\pi/3) \end{bmatrix} \begin{bmatrix} i_a \\ i_b \\ i_c \end{bmatrix} \quad (10)$$

where i_a, i_b, and i_c are the three-phase stator currents and i_d, i_q are the two-phase d-q axis currents. θ is the angle between the d-axis and the a-axis.

After obtaining the two-phase currents, a PI controller is used to calculate the reference current i_{qref} based on the error between the reference speed w_{ref} and the actual speed w of the motor. The PI controller output is given by:

$$i_{qref} = K_p(w_{ref} - w) + K_i \int_0^t (w_{ref} - w)dt \quad (11)$$

where K_p and K_i are the proportional and integral gains of the PI controller, respectively.

The MPC function then takes these reference values along with the current values of i_d, i_q, w, Time(t), and θ as inputs. It also requires the stator phase resistance (R), armature inductance (L), flux linkage (λ), Pole pairs (p) and DC link voltage (V_{dc}) to be provided for the function to be built. In order to create a cost matrix, the function initializes the possible combinations of switching states (S) for the three-phase inverter. Each combination of the switching states is stored in (S_a, S_b, S_c) variables [15].

Consequently, the function calculates the three-phase voltage values (V_{inva}, V_{invb}, V_{invc}) based on V_{dc} and the phase states using the following equations:

$$V_{inva} = \frac{V_{dc} \cdot (2 \cdot S_a - S_b - S_c)}{3} \quad (12)$$

$$V_{invb} = \frac{V_{dc} \cdot (2 \cdot S_b - S_a - S_c)}{3} \quad (13)$$

$$V_{invc} = \frac{V_{dc} \cdot (2 \cdot S_c - S_b - S_a)}{3} \quad (14)$$

The voltage values are then used to calculate the quadrature and direct components of the stator voltage, v_q and v_d, using the following equations:

$$v_q = \frac{2}{3}\left[(V_{inva} \cdot \cos(w \cdot t + \theta \cdot p)) + (V_{invb} \cdot \cos(w \cdot t + \theta \cdot p + \frac{4\pi}{3})) + (V_{invc} \cdot \cos(w \cdot t + \theta \cdot p + \frac{2\pi}{3}))\right] \quad (15)$$

$$v_d = \frac{2}{3}\left[(V_{inva} \cdot \sin(w \cdot t + \theta \cdot p)) + (V_{invb} \cdot \sin(w \cdot t + \theta \cdot p + \frac{4\pi}{3})) + (V_{invc} \cdot \sin(w \cdot t + \theta \cdot p + \frac{2\pi}{3}))\right] \quad (16)$$

Using these voltage values and the current values, the MPC function then calculates the predicted values of the quadrature and direct components of the stator current, i_{qp} and i_{dp}, using the following equations:

$$i_{dp} = (1 - \frac{R \cdot T_s}{L}) \cdot i_d + \frac{T_s \cdot w}{L} \cdot i_q + \frac{v_d \cdot T_s}{L} \quad (17)$$

$$i_{qp} = (1 - \frac{R \cdot T_s}{L}) \cdot i_q - \frac{T_s \cdot w}{L} \cdot i_d - \frac{\lambda \cdot w \cdot T_s}{L} + \frac{v_q \cdot T_s}{L} \quad (18)$$

where R is the motor resistance, L is the motor inductance, λ is the motor mutual inductance, and T_s is the sampling time.

The MPC function calculates a cost function for each of the eight possible combinations of phase states (S_a, S_b, S_c) and chooses the combination that minimizes the cost function. The cost function is calculated using the following equation:

$$cost(i) = i_{dp}^2 + (i_{qref} - i_{qp})^2 \quad (19)$$

where i is the index of the phase state combination, i_{dref} and i_{qref} are the reference current values.

After evaluating the cost function, the selection process determines the most suitable switching states, which are then fed as pulses to the three-phase inverter. This strategic configuration enables effective control of the PMSM, maximizing its high-speed capability and efficiency.

TABLE III
SIMULATION PARAMETERS

Parameter	Value
Simulation run time	50 s
Sampling period	20 μs
Li-ion Battery SoC & Charge Level of SCs	**Case 1:** Battery = 50%, SC = 81.44% **Case 2:** Battery = 50%, SC = 76.8% **Case 3:** Battery = 25%, SC = 81.44% **Case 4:** Battery = 25%, SC = 76.8%
Time constant	0.05 s
Rate limit	45000
DC-Link Voltage	300 V
Pole pairs	4
PMSM Stator phase resistance	0.0918 Ω
Armature inductance	0.975 mH
Flux linkage	0.1688

III. RESULTS AND DISCUSSION

The proposed HESS and PMSM control model were designed and analyzed in MATLAB/Simulink software. Due to the complexity of the model, the simulation was conducted for 50 seconds only. The simulation parameters and the corresponding values have been listed in Table III.

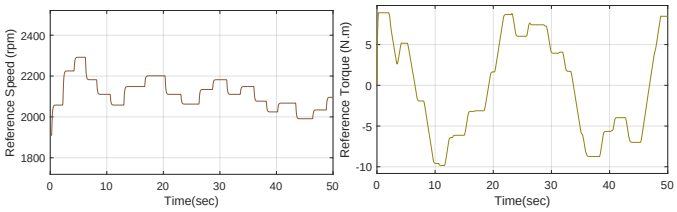

(a) (b)

Fig. 4. The required (a) rotational speed and (b) torque for the EV at dynamic conditions.

The MPC loop receives a variable reference rotational speed of the PMSM, ranging from 1990 rpm to 2300 rpm, as depicted in Fig. 4a. Additionally, the reference torque supplied to the PMSM ranges from -10 N.m to 10 N.m as shown in Fig. 4b. While observing Fig. 5, it is evident that the actual rotational speed of the PMSM adeptly tracks the reference speed as desired.

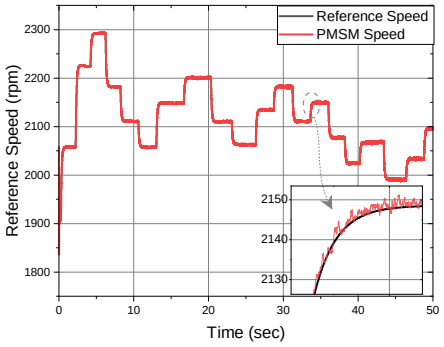

Fig. 5. Reference and actual speed of the PMSM.

Fig. 6a illustrates the power profile of the PMSM, with positive values indicating power consumption and negative values representing regenerative power generated by the PMSM. The proposed HESS supplies the fluctuating power profile required by the PMSM, as shown in Fig. 6b. The battery, serving as the primary energy storage, meets the power requirements with a smooth and consistent profile, as depicted in Fig. 6c. Conversely, the power profile of the SCs in Fig. 6d demonstrates its ability to handle fluctuations in power demand, thereby extending the overall battery life.

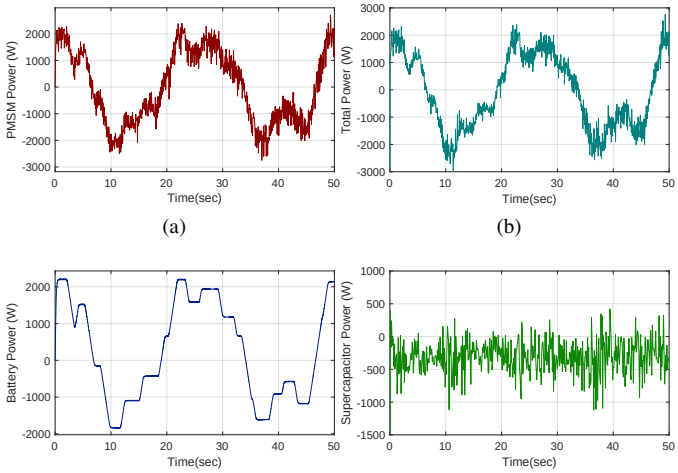

(a) (b)

(c) (d)

Fig. 6. Power profile: (a) PMSM (b) Total power (C) Battery and (d) SCs.

The voltage characteristics are illustrated in Fig. 7a, where the battery voltage fluctuates due to the charging and discharging processes. The SC terminal voltage remains stable at approximately 300V, contributing to the stabilization of the DC link voltage. The current profile of both the battery and SC, as shown in Fig. 7b, closely follows the power variations.

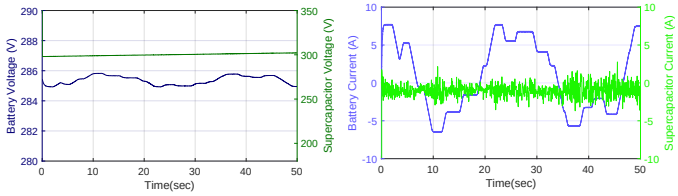

(a) (b)

Fig. 7. Battery and SC: (a) Voltage profile and (b) Current profile.

Fig. 8a presents the SoC profile of the Li-ion battery. Initially, from 0 to 8 seconds, the SoC decreases, indicating the battery discharging to meet the PMSM power demands. Subsequently, in the following 10 seconds, the SoC gradually increases, indicating the battery receiving power from the synchronous machine regeneratively. A comparison between Case 1 and Case 2 in Fig. 8a justifies the battery SoC experiencing a faster decline in the latter case. This can be attributed to the battery simultaneously charging the SCs also, leading to a higher discharge rate. When comparing Case 1 and Case 3 in Fig. 8b, a similar trend can be observed which demonstrates a faster decrease in the charge level for the SCs.

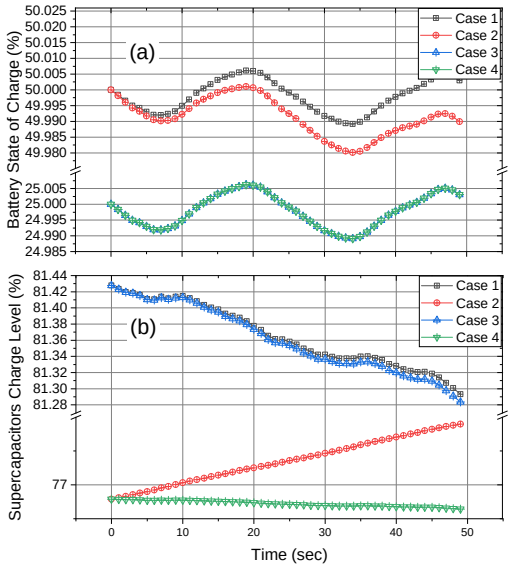

Fig. 8. Comparison of four cases: (a) Battery SoC and (b) SC charge level.

Fig. 9a exemplifies the stator current, which exhibits changes in amplitude corresponding to torque and speed requirements. The stator current also reveals high ripple caused by the electrical torque generated by the PMSM. The real-time efficiency of the model, as portrayed in Fig. 9b, exhibits consistently high values exceeding 98% for both PMSM energy consumption and regenerative energy. However, minor fluctuations are observed in the graph, primarily due to rapid switching between the motor and generator modes of the PMSM.

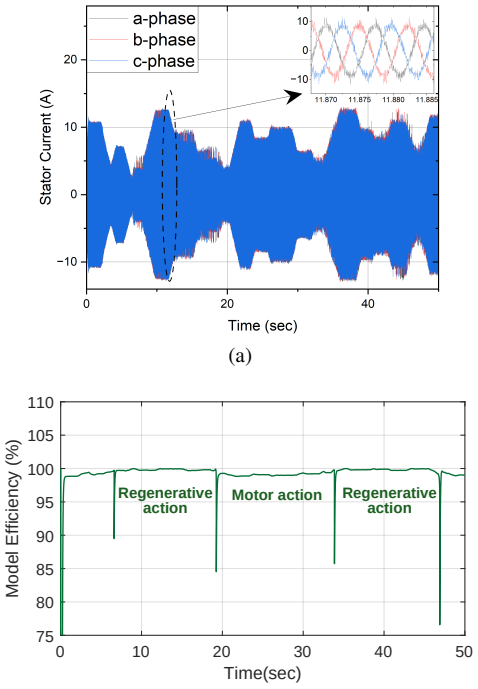

Fig. 9. (a) PMSM stator current and (b) Real-time model efficiency.

IV. Conclusion

This paper presents the design and analysis of a rule-based Energy Management System (EMS) for a semi-active Hybrid Energy Storage System (HESS) combining batteries and SCs. The proposed EMS is specifically tailored for EVs, ensuring optimal energy management and efficiency. Furthermore, the Model Predictive Control (MPC) strategy has been utilized to control the speed of the PMSM for the proposed model. The battery seamlessly caters the smoother power demands, while the SCs adeptly manages the irregular fluctuations, resulting in extended battery life and elevated system performance. The model efficiency has been measured in real-time surpassing an impressive value of 98%. The comprehensive design and exceptional efficiency underpin the system's strong suitability for practical EV applications, making it an enticing prospect for sustainable transportation.

References

[1] Santos, Georgina. "Road transport and CO2 emissions: What are the challenges?." Transport Policy 59 (2017): 71-74.

[2] Hasan, Md Arif, et al. "Emissions from the road transport sector of New Zealand: Key drivers and challenges." Environmental Science and Pollution Research 26 (2019): 23937-23957.

[3] Sadeq, Taha, et al. "Optimal control strategy to maximize the performance of hybrid energy storage system for electric vehicle considering topography information." IEEE Access 8 (2020): 216994-217007.

[4] Shen, Junyi, Serkan Dusmez, and Alireza Khaligh. "Optimization of sizing and battery cycle life in battery/ultracapacitor hybrid energy storage systems for electric vehicle applications." IEEE Transactions on industrial informatics 10.4 (2014): 2112-2121.

[5] Ranjan, Alok, and Sanjay B. Bodkhe. "Modified energy management strategy for hess in electric vehicle." 2021 9th IEEE International Conference on Power Systems (ICPS). IEEE, 2021.

[6] Zhang, Lijun, et al. "A real-time energy management and speed controller for an electric vehicle powered by a hybrid energy storage system." IEEE Transactions on Industrial Informatics 16.10 (2020): 6272-6280.

[7] Bai, Yunfei, et al. "Optimal design of a hybrid energy storage system in a plug-in hybrid electric vehicle for battery lifetime improvement." IEEE Access 8 (2020): 142148-142158.

[8] Tian, Zhiyong, et al. "Real-time charging station recommendation system for electric-vehicle taxis." IEEE Transactions on Intelligent Transportation Systems 17.11 (2016): 3098-3109.

[9] Kim, Jaewan, Jinwoo Oh, and Hoseong Lee. "Review on battery thermal management system for electric vehicles." Applied thermal engineering 149 (2019): 192-212.

[10] Hannan, Mahammad A., et al. "State-of-the-art and energy management system of lithium-ion batteries in electric vehicle applications: Issues and recommendations." IEEE Access 6 (2018): 19362-19378.

[11] Aruna, P., and Prabhu V. Vasan. "Review on energy management system of electric vehicles." 2019 2nd International Conference on Power and Embedded Drive Control (ICPEDC). IEEE, 2019.

[12] F. Chen, C. Ge, D. Tang, S. Ding, and X. Gong, "Energy management and nonlinear control strategy of hybrid energy storage system for electric vehicle," Energy Reports, vol. 8, pp. 11161–11173, Nov. 2022, doi: https://doi.org/10.1016/j.egyr.2022.08.250.

[13] M. -E. Choi, S. -W. Kim and S. -W. Seo, "Energy Management Optimization in a Battery/Supercapacitor Hybrid Energy Storage System," in IEEE Transactions on Smart Grid, vol. 3, no. 1, pp. 463-472, March 2012, doi: 10.1109/TSG.2011.2164816.

[14] S. Hu, Z. Liang, W. Zhang and X. He, "Research on the Integration of Hybrid Energy Storage System and Dual Three-Phase PMSM Drive in EV," in IEEE Transactions on Industrial Electronics, vol. 65, no. 8, pp. 6602-6611, Aug. 2018, doi: 10.1109/TIE.2017.2752141.

[15] P. Golchoubian and N. L. Azad, "Real-Time Nonlinear Model Predictive Control of a Battery–Supercapacitor Hybrid Energy Storage System in Electric Vehicles," in IEEE Transactions on Vehicular Technology, vol. 66, no. 11, pp. 9678-9688, Nov. 2017, doi: 10.1109/TVT.2017.2725307.